The 11th Canadian Conference on Earthquake Engineering
Canadian Association for Earthquake Engineering

SEISMIC PERFORMANCE EVALUATION OF BRIDGE PIER REINFORCED WITH DIFFERENT TYPES OF SHAPE MEMORY ALLOY REBAR

AHM Muntasir BILLAH
PhD Candidate, School of Engineering, The University of British Columbia, Canada
muntasir.billah@ubc.ca

M Shahria ALAM
Associate Professor, School of Engineering, The University of British Columbia, Canada
Shahria.alam@ubc.ca

ABSTRACT: The distinct thermomechanical properties and flag shape hysteresis of Shape Memory Alloys (SMAs) make them an ideal candidate for the development and design of various structural components for civil infrastructures. Numerous experimental and numerical studies proved the efficiency of SMA reinforced structures in seismic regions. Most of the applications have been focusing on the use of Ni-Ti alloy while very few focused on the application of the alloys such as Cu-based SMAs and Fe-based SMAs. Although Ni-Ti SMA shows large recoverable strain, good superelasticity and exceptionally good resistance to corrosion, extremely high cost of Ni-Ti SMA and machinability restrict its large scale applications. Many different types of SMAs have been developed recently that have huge potentials for smart structural applications, such as in highway bridges. In this study, Ni-Ti, Fe- based and Cu-based SMAs are used in bridge piers for evaluating their performance under seismic loading. Using incremental dynamic analysis, the performance of different SMA reinforced bridge piers are evaluated in terms of maximum and residual drift. Different seismic performance limit states for each type of the studied bridge piers were identified and the efficacy of different SMA rebars in improving the performance of bridge piers were discussed in detail to better assist design engineers to select/design the appropriate SMA type considering the desired performance objectives.

1. Introduction

Current seismic design guidelines, followed in North America (CHBDC 2014, AASHTO LRFD 2012) and Europe (EC8-2), allow bridges other than life line bridges to undergo large inelastic deformation while maintaining the load carrying capacity without being completely collapsed during a design level earthquake. However, past experiences (Kobe 1995, Northridge 1994) have shown that bridges undergoing large lateral drift are prone to large residual deformation which renders the bridges to be unusable and require major rehabilitation or replacement. In order to maintain the structural integrity and functionality of a bridge after an earthquake, it is necessary that the bridge components avoid excessive residual deformation or permanent damage (Kawashima et al. 1998). Bridge pier is one of the most critical components of a bridge since the overall seismic response of a bridge is largely dependent on the response of the piers. The extent of residual or permanent deformation sustained by the bridge piers prescribes the likelihood of allowing traffic over the bridge and dictates the amount of repair works and expected loss. Observations from recent earthquakes (Kobe 1995, Northridge 1994) and a desire to develop innovative structural systems with improved post-earthquake functionality have motivated researchers to pioneer and test different novel structural systems. For example, to reduce the residual displacement of bridge piers, researchers have recommended innovative unbonded post-tensioned RC

bridge columns (Hewes and Priestley 2002) and Shape Memory Alloy (SMA) reinforced concrete (RC) bridge piers (Billah and Alam 2014).

Over the last few years, researchers have experimentally and numerically investigated the potential application of shape memory alloys in bridge piers and found promising results (Billah and Alam 2014, Cruz and Saiidi 2012). However, all the previous studies were focused on the application of Ni-Ti SMA while few study focused on Cu-based SMA (Shrestha et al. 2015). Recently, researchers have come up with various Fe-based and Cu- based low cost SMAs which hold great potential for application in bridge piers. Tanaka et al. (2010) developed a ferrous polycrystalline SMA (Fe-Ni-Co-Al-Ta-B) which has a very high superelastic strain range of over 13% at room temperature. This SMA has approximately 20 times higher superelasticity than Fe-Ni-Co-Ti alloy and almost double that of conventional Ni-Ti alloy. This Fe-based SMA has extremely high ductility, greater strength, and also energy dissipation capacity several times higher than that of commercially available Ni-Ti SMA. In this study, one nickel–titanium, one Cu-based, and one Fe- based shape memory alloys, have been selected for use in bridge piers.

The objective of this study is to compare the seismic performance of concrete bridge piers reinforced with different types of SMA rebar in the plastic hinge region. The performance of the bridge piers are compared in terms of different performance criteria, i.e., cracking, yielding, spalling and crushing.

2. Design and Geometry of Bridge Piers

This section briefly describes the design and configurations of different SMA-RC bridge piers used in this study. Since SMA is a costly material, it is only used in the bottom plastic hinge region of the bridge piers. Three different SMAs are used in this study to compare the performance of different SMA-RC bridge piers. The bridge pier is assumed to be located in Vancouver, BC and was seismically designed following Canadian Highway Bridge Design Code (CHBDC 2010). Figure 1 shows the cross section and elevation of the bridge pier. The diameter of all the columns was fixed to be 1.83 m; the columns were reinforced with 48 longitudinal reinforcement of different diameter bars for different SMAs and 16 mm-diameter steel spirals at 76 mm pitch. The height of the pier is 9.14m with an aspect ratio of 5 which ensured the flexure dominated behavior. Different diameter bars were used for different SMAs since different SMAs have different elastic modulus and yield strength. Although SMA does not have a yielding process, “yield” is being used to refer to the initiation of phase transformation of SMA and the yield strain was calculated by deviding the austenite to martensite starting stress (*fy*) by the elastic modulus (*E*). Three different SMA rebars as shown in Table 1 are used to design the different bridge piers.

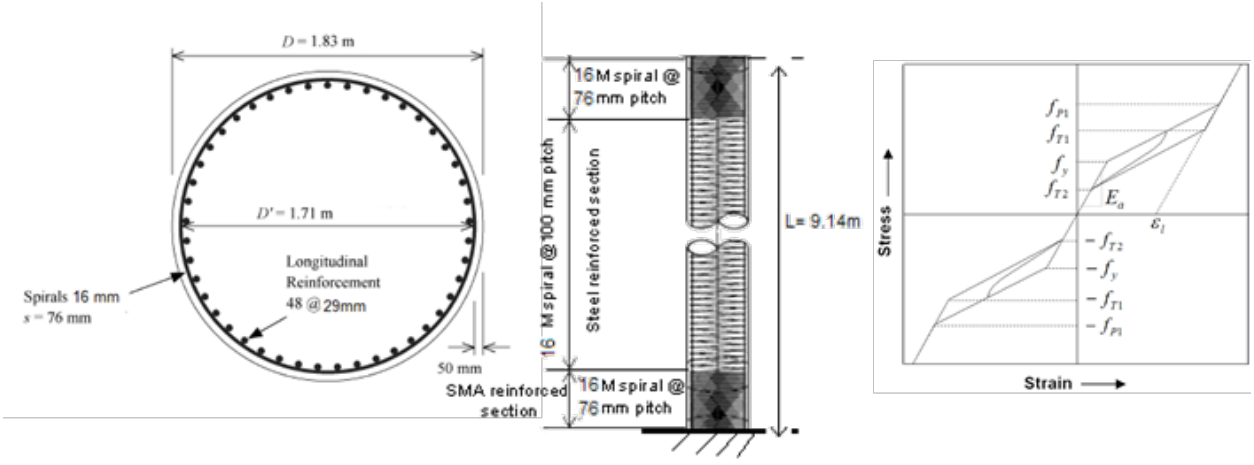

Fig. 1- (a) Cross section, (b) elevation of SMA reinforced concrete bridge pier and (c) stress-strain relation of SMA rebar

Table 1- Properties of different types of SMA

	Alloy	εs (%)	E (GPa)	fy (MPa)	f_{p1} (MPa)	f_{T1} (MPa)	f_{T2} (MPa)	Ref
SMA-1	$NiTi_{45}$	6	62.5	401.0	510	370	130	Alam et al. 2008
SMA-2	FeNCATB	13.5	46.9	750	1200	300	200	Tanaka et al. 2010
SMA-3	CuAlMn	9	28	210.0	275.0	200	150	Shrestha et al. 2013

f_y (austenite to martensite starting stress); f_{P1}(austenite to martensite finishing stress); f_{T1}(martensite to austenite starting stress); f_{T2}(martensite to austenite finishing stress) , ε_s (superelastic plateau strain length); and E (modulus of elasticity)

The bridge piers are designated as SMA-RC-1 (reinforced with SMA-1), SMA-RC-2 (reinforced with SMA-2), and so on. SMA-RC-1 is reinforced with 48-28M SMA-1 bars, SMA-RC-2 is reinforced with 48-20M SMA-2 bars, and SMA-RC-3 is reinforced with 48-35M SMA-3 bars, respectively. The sizes of the rebars were selected in such a way that the axial forces developed in the rebar are almost similar. The bridge piers are designed in such a way that they have comparable moment capacities. Figure 2a shows the moment-curvature response of different SMA-RC sections. From this figure it is evident that all the sections have similar initial stiffness and comparable moment capacity. Since SMA-1 has higher elastic modulus SMA-RC-1 showed higher initial stiffness which is 1.78 and 2.21 times higher than that of SMA-SMA-RC-2 and SMA-RC-3 respectively. Moment-curvature response of all the sections revealed that this design process led to comparable moment capacities for the five different SMA reinforced bridge piers. The elastic periods of the SMA-RC-1, SMA-RC-2, and SMA-RC-3 were calculated as 0.513 sec, 0.514, and 0.515 sec, respectively which were close and expected to attract similar earthquake forces. Figure 2b shows the pushover response curves for the five different SMA-RC bridge piers. From this figure it can be observed that all the bridge piers have similar stiffness and load carrying capacity.

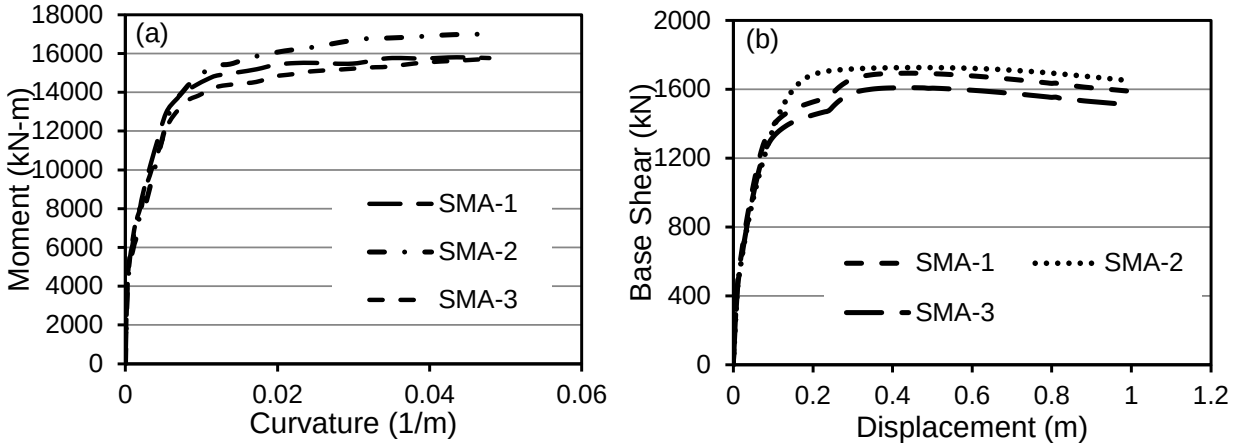

Fig. 2- (a) Moment curvature relationship of RC sections with different types of SMA and (b) Static pushover curves for bridge piers reinforced with different types of SMA

The material properties of concrete and steel rebar used in the bridge piers are summarized in Table 2. In the SMA-RC bridge piers, SMA was used as longitudinal reinforcement only at the plastic hinge region. In the remaining part, steel rebars were used as reinforcement. The plastic hinge length, *Lp* was calculated according to the Paulay and Priestley (1992) equation:

$$Lp = 0.08\,L + 0.022 d_b f_y \quad (1)$$

where, L is the length of the member in mm, d_b represents the bar diameter in mm and f_y is the yield strength of the rebar in MPa.

Table 2- Material properties for SMA-RC bridge pier

Material	Property	
Concrete	Compressive Strength (MPa)	42.4
	Corresponding strain	0.0029
	Tensile strength (MPa)	3.5
	Elastic modulus (GPa)	23.1
Steel	Elastic modulus (GPa)	200
	Yield stress (MPa)	475
	Ultimate stress (MPa)	692
	Ultimate strain	0.14
	Plateau strain	0.016

3. Analytical Modeling of Bridge Piers

In this study, a fiber element based nonlinear analysis program SeismoStruct (Seismosoft, 2014) has been employed for modeling different SMA-RC bridge piers. Incremental dynamic analyses (IDA) have been performed to compare the seismic performance of SMA-RC bridge piers. The program has the ability to determine the large displacement behaviour and the collapse load of framed structures accurately under either static or dynamic loading, while taking into account both geometric nonlinearities and material inelasticity. The bridge piers were modelled with 3D inelastic beam–column element (force based element), with circular section for the piers; the constitutive laws of the reinforcing steel and concrete were, respectively, the Menegotto–Pinto (1973) and Mander et al. (1988) models. The superelastic SMA model developed by Auricchio and Sacco (1997) has been employed for modeling SMA using the parameters provided in Table 1.

The accuracy of the program in predicting the seismic response of bridge structures has been demonstrated by several researchers through comparisons with experimental results (Alam et al. 2009, Billah and Alam, 2013). Figure 3 shows the comparison of experimental and analytical results from two different studies using two different SMAs. Figure 3a shows the comparison of shake table test results and analytical results of a SMA-steel RC bridge pier where SMA was particularly used in the plastic hinge region. The numerical results obtained from SeismoStruct could predict the experimental result of Saiidi and Wang (2006) accurately where the variations were only 5.6%, 6.1%, and 9.4% for base shear, tip displacement, and amount of energy dissipation, respectively. Figure 3b shows the load-rotation response of concrete beam reinforced with Cu-Al-Mn SMA (SMA-3) in the mid span under four point reverse cyclic loading (Shrestha et al. 2013). From this figure it is evident that the adopted analytical model was capable of predicting the experimental response very well where the variations were only 3.4% and 5.9% for maximum force and beam rotation, respectively.

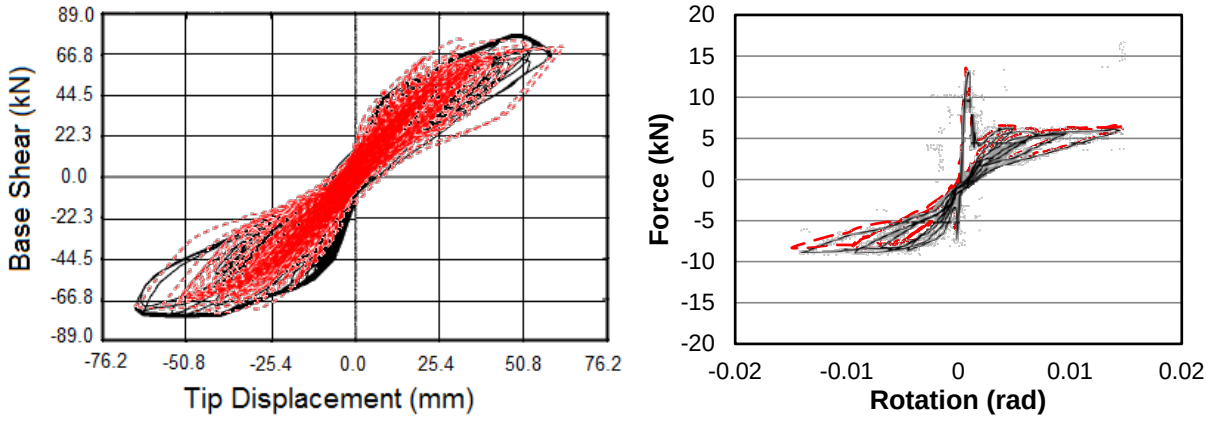

Fig.3- Comparison of experimental and numerical results (a) SMA-RC (SMA-1) bridge pier (b) SMA-RC (SMA-4) beam

4. Performance Assessment Approach

Incremental dynamic analysis (IDA) was employed to evaluate the seismic performance of different SMA-RC bridge piers. IDA is a useful method for more detailed seismic performance predictions of structures subjected to different seismic excitation levels (Vamvatsikos and Cornell, 2002). In IDA, the analytical structural model is subjected to numerous inelastic time history analyses performed using one or a set of ground motion record(s), each scaled (up or down) to study different seismic intensity levels while tracking the response of the structure (e.g., displacements, accelerations, etc.). This procedure of scaling and time history analysis is repeated until dynamic instability in the form of large drifts occurs, indicating structural collapse. In addition to collapse, the IDA results can be used for seismic performance assessment at different damage states (Tehrani and Mitchell 2013). Usually the IDA results are presented in terms of an intensity measure (IM) and an engineering demand parameter (EDP). Commonly used IMs in IDA analysis are PGA, PGV, and 5% damped Spectral Acceleration at the structure's first-mode period (Sa (T_1,5%)). In this study, Sa (T_1,5%) is used as the IM since it is recommended by different guidelines (FEMA-P695) and researchers (Vamvatsikos and Cornell 2002, Tehrani and Mitchell 2013).

4.1. Selection of ground motions

The incremental dynamic analyses were carried out using the 10 selected ground motions as shown in Table 3. These ground motion records were obtained from the PEER NGA ground motion database (2011). These accelerograms were chosen such that they represent the seismic characteristics of the site of the structure. The recent edition of Canadian Highway Bridge Design Code (CHBDC 2014) requires that highway bridges should meet target performance levels under seismic ground motions with different return periods. In this study, three different levels of seismic ground motions were considered according to CHBDC 2014 (CSA S6-14). These records correspond to three different hazard levels with a 2%, 5%, and 10% probability of exceedance in 50 years. The respective return periods are 2475 years, 975 years, and 475 years. For each hazard level, 10 ground motions shown in Table 3 were used. The selected ground motions were scaled to specific hazard levels using SeismoMatch (Seismosoft 2013). This software is able to adjust any ground motion accelerograms to match a specific design response spectrum using wavelet algorithm proposed by Abrahamson (1992) and Hancock et al. (2006). The mean spectra and the target spectra corresponding to different hazard levels are shown in Figure 4.

Table 3- Selected earthquake ground motion records

No	Event	Year	Record Station	M	R(km)	PGA (g)
1	Imperial Valley	1979	El Centro Array#11	6.5	21.9	0.36
2	Imperial Valley	1979	Chihuahua	6.5	28.7	0.254
3	Kobe	1995	Takatori	6.9	4.3	0.56
4	Kobe	1995	JMA	6.9	3.4	0.77
5	Loma Prieta	1989	Holister South & Pine	6.9	28.8	0.371
6	Loma Prieta	1989	16 LGPC	6.9	16.9	0.605
7	Nothridge	1994	Rinaldi	6.7	7.5	0.87
8	Nothridge	1979	Olive View	6.7	6.4	0.721
9	Superstition Hill	1987	Wildlife liquefaction array	6.7	24.4	0.134
10	Superstition Hill	1987	Wildlife liquefaction array	6.7	24.4	0.132

4.2. Characterization of performance limits

The seismic responses of three different SMA-RC bridge piers are compared using the 10 selected ground motions scaled to different hazard levels. In order to compare their relative performance it is necessary to define some performance limits based on which the comparative response can be evaluated. To implement such procedures, it is necessary to define damage in terms of engineering performance criteria. In this study, the performances of the three bridge piers are compared in terms of maximum drift and residual drift. Performance evaluation need to be conducted in such a way that it results in more predictable seismic performance over the full range of earthquake demand (Hose et al. 2000). Since very limited experimental results are available on SMA-RC bridge piers and all of them focus

on Ni-Ti SMA, performance-based damage states for SMA-RC bridge piers developed by Billah and Alam (2015) has been considered in this study. Billah and Alam (2015) developed performance-based damage states for five different SMA-RC bridge piers in terms of maximum and residual drift as well as considering different seismic hazard levels. These damage states were developed based on extensive numerical analysis and the details can be found in Billah and Alam (2015). Table 5 shows the maximum and residual drift damage states adopted in this study and the definition of associated functional level.

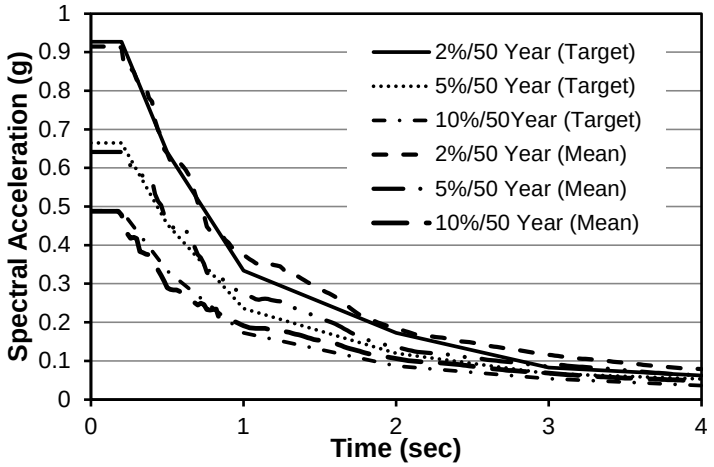

Fig.4- Design and mean response spectrum of 10 records used for IDA analysis matching the three different CHBDC spectrum (2%, 5%, and 10% in 50 years)

Table-5 Maximum drift damage states of SMA-RC bridge pier

Damage State	Performance Level	Functional Level	Description	Maximum Drift (%)			Residual Drift, RD (%)
				SMA-RC-1	SMA-RC-2	SMA-RC-3	
Slight (DS=1)	Cracking	Fully Operational	Onset of cracking	0.28	0.28	0.28	0.33
Moderate (DS=2)	Yielding	Operational	Theoretical first yield of longitudinal rebar	1.68	2.28	1.74	0.62
Extensive (DS=3)	Initiation of Local Mechanism	Life safety	Onset of concrete spalling	2.66	1.64	2.52	0.87
Collapse (DS=4)	Strength Degradation	Collapse	Crushing of core concrete	5.05	7.65	5.56	1.22

4.2.1. Maximum Drift

To evaluate the performance of three different SMA-RC bridge piers IDA curves were developed using Sa (T1,5%) as the IM and maximum drift (%) as the DM. Figures 5a,b,c show the IDA curves for the three SMA-RC bridge piers obtained using the selected ground motions. Since there are number of ground motions used in the IDA scaled to different hazard levels, the results are summarized using the DM given IM (i.e., DM|IM) percentiles (Vamvatsikos and Cornell, 2002). The IDA results are summarized in median (50% percentile), 16%, and 84% percentiles. With the assumption of a lognormal distribution of maximum drift ratio as a function of Sa(T1), the median (i.e., 50% percentile) is the natural 'central value' and the 84%, 16% percentiles correspond to the median times $e^{\pm dispersion}$, where 'dispersion' is the standard deviation of the logarithms of the values (Jalayer and Cornell, 2003).

For performance assessment in terms of the maximum drift limits shown in Table 5, the limit states are defined in the IDA curves. The limit states on the IDA curves are defined in terms of DM based rule (Vamvatsikos and Cornell, 2002) which indicates that if the DM value exceeds a certain limit (e.g., the drift capacity at different limit states such as DS-2, DS-3, DS-4, etc.) then the limit state is exceeded. Figure 5a shows the IDA curves for the SMA-RC-1 along with the collapse threshold (solid vertical line) and collapse drift limit (dashed vertical line) obtained from IDA. From figure 5a it can be seen that the SMA-RC-1 could withstand a median maximum drift of 4.94% just before collapse (dashed vertical line), compared to 5.05% collapse drift limit presented in Table 5. From figure 5b, it can be observed that SMA-RC-2 could withstand a median maximum drift of 7.35% just before collapse (dashed vertical line), compared to 7.65% collapse drift limit presented in Table 5. Similar observation can be made for SMA-RC-3 which collapsed at a median maximum drift of 5.25% as compared to the collapse drift limit of 5.56%.

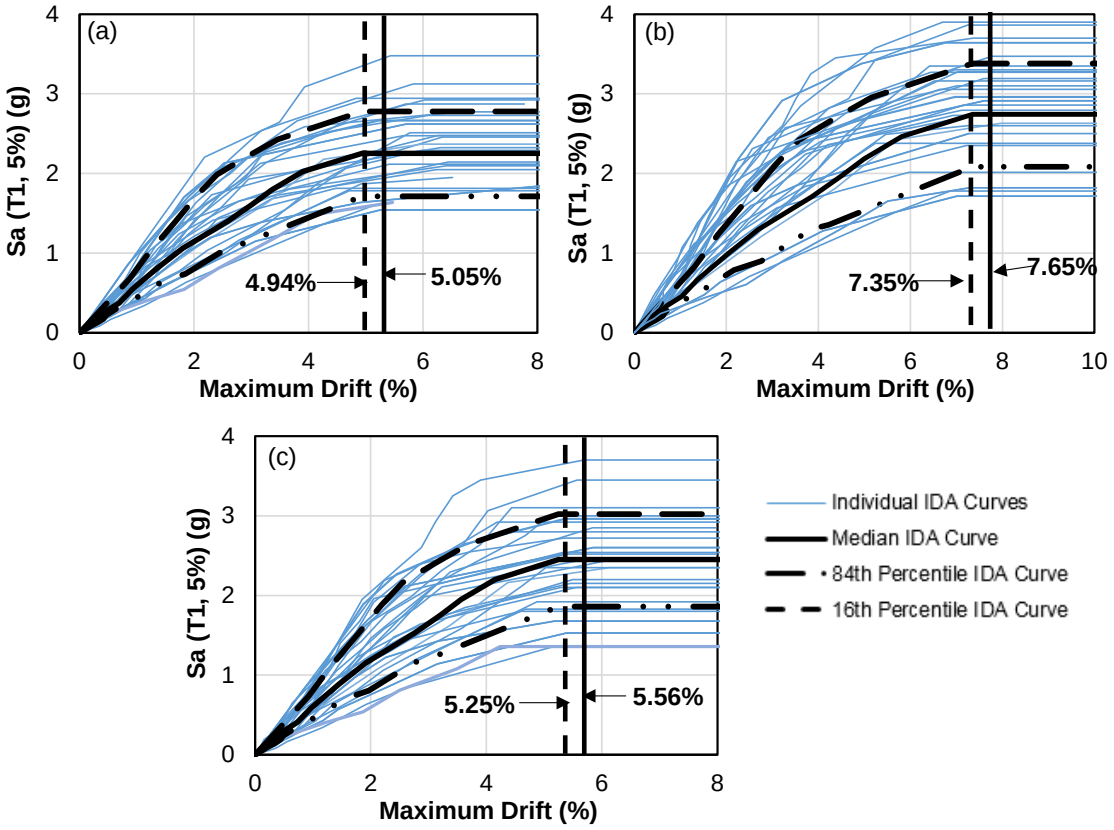

Fig.5- IDA curves for maximum drift (a) SMA-RC-1, (b) SMA-RC-2, (c) SMA-RC-3

Table 6 compares the median Sa for different damage states for different SMA-RC piers. Table 6 does not compare the median Sa for DS-1 as all the piers experiences DS-1 at same intensity of ground motions. From table 6, it is evident that except for DS-3, SMA-RC-2 performed better as compared to other two bridge piers. From table 6 it can be observed that the median Sa at yielding (DS-2) is 1.18g for SMA-RC-2 which is 18% and 12% higher than that of SMA-RC-1 and SMA-RC-2, respectively. This can be attributed to the very high yield strength of SMA-3 as compared to other SMAs. On the other hand, the median Sa at spalling (DS-3) is 0.94g for SMA-RC-2 which is 37% and 35% lower than that of SMA-RC-1 and SMA-RC-2, respectively. This can be attributed to the drift limit associated with DS-3. From Table 5, it can be seen that SMA-RC-2 has comparatively lower drift limits at DS-3, as compared to other two piers. A comparison of the performance of the three bridge piers provide an insight into the relative effectiveness of different SMA reinforced bridge piers. A comparison of the collapse drift (%) of the three bridge bent revealed that the SMA-RC-3 could sustain higher drift before collapse under different hazard levels as compared to the SMA-RC-1 and SMA-RC-2.

Table-6 Comparison of median Sa(T1,5%) (g) at different damage states (Maximum Drift)

	SMA-RC-1			SMA-RC-2			SMA-RC-3		
	16%	Median	84%	16%	Median	84%	16%	Median	84%
DS-2	0.74	0.96	1.40	0.86	1.18	1.74	0.78	1.04	1.43
DS-3	1.09	1.48	1.82	0.72	0.94	1.12	1.03	1.46	1.75
DS-4	1.71	2.26	2.78	2.08	2.73	3.38	1.86	2.44	3.02

4.2.2. Residual Drift

Residual drift has been considered as one of the significant performance indicators for seismic performance assessment of structures (Ramirez and Miranda 2012). Although residual drift dictates the post-earthquake functionality of highway bridges, no other design guidelines except the Japanese code for highway bridge design (2006) provide any residual drift limit of bridge piers. In this study, residual drift damage states proposed by Billah and Alam (2015) are used to compare the performance of different SMA-RC bridge piers.

Figure 6 shows the comparative performance of three bridge piers in terms of residual drift. From the figure it can be seen that the bridge pier reinforced with SMA-2 could undergo large residual drift (1.32%) before collapse which is 10% and 6% higher than the SMA-RC-1 and SMA-RC-3 pier, respectively. Interestingly, except SMA-RC-1, other two SMA-RC piers exceeded the collapse drift limit (1.22%). Table 7 shows the comparative performance of different SMA-RC piers in reaching different damage states in terms of median Sa. From Table 7, it can be observed that, the median collapse Sa for SMA-RC-2 is 2.43g which is 12% and 10% higher than that of SMA-RC-1 and SMA-RC-3, respectively. In all damage states, SMA-RC-2 performed better than other two SMA-RC piers. This can be attributed to the significantly higher superelastic strain and yield strength of SMA-2.

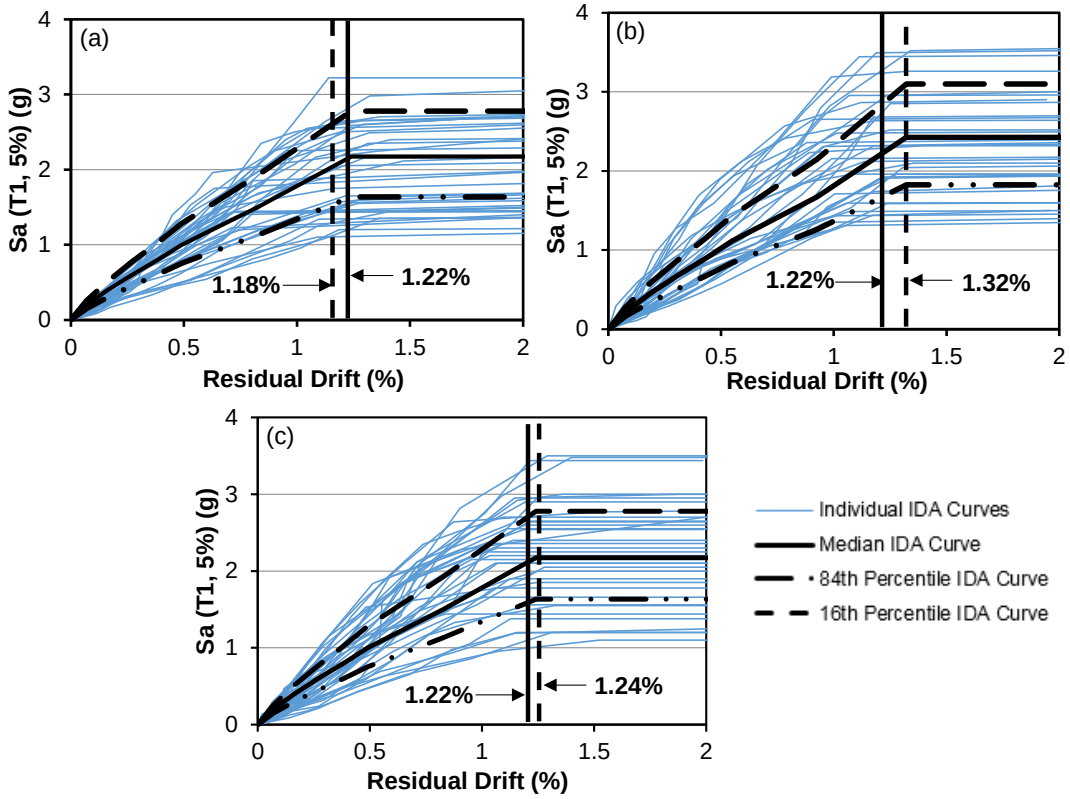

Fig.6- IDA curves for residual drift (a) SMA-RC-1, (b) SMA-RC-2, (c) SMA-RC-3

Table-7 Comparison of median Sa (T1,5%) (g) at different damage states (Residual Drift)

	SMA-RC-1			SMA-RC-2			SMA-RC-3		
	16%	Median	84%	16%	Median	84%	16%	Median	84%
DS-1	0.49	0.65	0.87	0.57	0.72	0.94	0.53	0.69	0.90
DS-2	0.92	1.22	1.58	1.05	1.37	1.69	0.94	1.26	1.60
DS-3	1.14	1.50	1.89	1.24	1.62	2.07	1.14	1.54	1.93
DS-4	1.61	2.13	2.75	1.82	2.43	3.10	1.64	2.17	2.78

5. Conclusions

Results from a comprehensive study on the seismic collapse capacity of concrete bridge piers reinforced with three different types of SMA rebars are presented in this paper. Calibrated analytical models of the studied bridge piers were subjected to ten different ground motions scaled to three different hazard levels with a 2%, 5%, and 10% probability of exceedance in 50 years. The seismic collapse capacities of the SMA-RC bridge piers were investigated through extensive series of IDA analyses considering maximum and residual drift as the demand parameter. This study provided an understanding on the failure capacity of different SMA-RC bridge piers when subjected to a wide variety of ground motions. Different seismic performance limit states for each type of the studied bridge piers were identified and the efficacy of different SMA rebars in improving the performance of bridge piers were discussed in detail to better assist design engineers to select/design the appropriate SMA type considering the desired performance objectives. Based on the results obtained, the following conclusions are drawn:

1. The EDPs considered in this study, i.e., maximum drift and residual drift, are shown to be well correlated with the intensity measure (Sa) considered in this study which provided a basis for a comparative seismic performance assessment.
2. Mechanical properties of different shape memory alloys, specifically the recovery strain, significantly affects the seismic performance of SMA reinforced concrete bridge piers in terms of both residual and maximum drift.
3. Except for DS-1(cracking), other three maximum drift damage states are significantly influenced by the type of SMA used. For DS-2 (yielding), the median Sa (T1, 5%) varies from 0.96g (SMA-RC-1) to 1.18 g (SMA-RC-2) and for DS-3 (spalling), median Sa (T1, 5%) varies from 0.94g (SMA-RC-2) to 1.48g (SMA-RC-1).
4. Effect of different SMA rebars are more pronounced when residual drift is considered as the demand parameter. Both SMA-RC-2 and SMA-RC-3, exceeded the collapse threshold of 1.22% while the collapse drift of SMA-RC-1 was 3.3% less than the collapse threshold..
5. In terms of residual drift, the SMA-RC-2 outperformed all other SMA-RC bridge piers at all damage states and significantly reduced the overall vulnerability of the bridge pier. This can be attributed to the higher superelastic strain and low residual strain of SMA-2.

6. Acknowledgements

Financial contribution of NSERC Canada is gratefully acknowledged.

7. References

Abrahamson, NA. “Non-stationary spectral matching”, *Seismological Research Letters*, 1992; 63(1):30.

Alam, M.S., Youssef. M.A. and Nehdi, M. “Analytical prediction of the seismic behaviour of superelastic shape memory alloy reinforced concrete elements.” *Engr. Struct.*, 30(12),2008, 3399-3411.

Alam, M.S., Youssef. M.A. and Nehdi, M. “Seismic performance of concrete frame structures reinforced with superelastic shape memory alloys.” *Smart Struct. and Syst.*, 5(5),2009: 565-585.

American Association of State Highway and Transportation Officials (AASHTO). (2011) “*AASHTO Guide Specifications for LRFD Seismic Bridge Design*,” 2nd ed., AASHTO, Washington, D.C.

Auricchio, F. and Sacco, E. “Superelastic shape-memory-alloy beam model.” *J Intelligent Materl Syst Struct*, 8(6), 1997,489–501.

Billah AHMM and Alam MS. “Performance based seismic design of concrete bridge pier reinforced with Shape Memory Alloy- Part 1: Development of Performance- Based Damage States.” Submitted in: ASCE *J. Struct. Eng.* 2015. 10pp.

Billah, A.H.M.M. and Alam, M.S. “Seismic fragility assessment of concrete bridge pier reinforced with superelastic Shape Memory Alloy.” Earthquake Spectra, in press: 2014, DOI: http://dx.doi.org/10.1193/112512EQS337M

Billah, A.H.M.M., Alam, M.S. and Bhuiyan, A.R. “Fragility analysis of retrofitted multi-column bridge bent subjected to near fault and far field ground motion.” *ASCE Journal of Bridge Engineering,* 18(10), 2013: 992-1004.

Canadian Standards Association. CAN/CSA-S6-10—“Canadian highway bridge design code.” *Canadian Standards Association*, Rexdale, Ontario, Canada,2010, 752 pp.

Canadian Standards Association. CAN/CSA-S6-14—“Canadian highway bridge design code.” *Canadian Standards Association*, Rexdale, Ontario, Canada, 2014, 894 pp.

Cruz, N.C. and Saiidi, M.S. “Shake-table studies of a four-span bridge model with advanced materials.” *J. Struct. Eng.*, *ASCE*, 138(2), 2012: 183–192.

EC8-2, (2008). Eurocode 8: Design of Structures for Earthquake Resistance—Part 2. *Seismic Design of Bridges*, European Committee for Standardization, Brussels, Belgium.

Hancock J, Watson-Lamprey J, Abrahamson NA, Bommer JJ, Markatis A, McCoy E, Mendis R. “An improved method of matching response spectra of recorded earthquake ground motion using wavelets.” *Journal of Earthquake Engineering*, 2006; **10**: 67–89.

Hewes, J. T., and Priestley, M. J. N. “Seismic design and performance of precast concrete segmental bridge columns.” *Report No. SSRP–2001/25*, Department of Structural Engineering, University of California, San Diego, 2002.

Jalayer F and Cornell CA. A technical framework for probability-based demand and capacity factor (DCFD) seismic formats. PEER-2003/08, Pacific Earthquake Engineering Research Center, 2003; University of California- Berkeley, Berkeley, CA.

Kawashima, K., MacRae, G., Hoshikuma, J. and Nagaya, K. “Residual displacement response spectrum.” *ASCE J. Struct. Engr*. 124(5), 1998: 523-530.

Mander, J.B., Priestley, M.J.N. and Park, R. (1988). Theoretical stress–strain model for confined concrete. *J. Struct. Eng.*, *ASCE*, 114(8):1804–26.

Menegotto, M. and Pinto, P.E. (1973). Method of analysis for cyclically loaded R.C. plane frames including changes in geometry and non-elastic behaviour of elements under combined normal force and bending. *Symposium on the resistance and ultimate deformability of structures acted on by well-defined repeated loads*, International Association for Bridge and Structural Engineering, Zurich, Switzerland, 1973; 15-22.

Paulay, T. and Priestley, M.N.J. (1992). Seismic design of reinforced concrete and masonry buildings. *New York: John Willey & Sons, Inc*.

Ramirez, C.M. and Miranda, E. (2012). Significance of residual drifts in building earthquake loss estimation. *Earthq. Eng Struct Dyn.,* 41: 1477-1493.

Saiidi, M.S. and Wang, H. (2006). Exploratory study of seismic response of concrete columns with shape memory alloys reinforcement. *ACI Struct. J.* 103(3): 435-42.

SeismoSoft. (2014). SeismoStruct - A computer program for static and dynamic nonlinear analysis of framed structures, V 7 [online], available from URL: www.seismosoft.com.

SeismoSoft, (2013). SeismoMatch - A computer program for adjusting ground motion data, V 2.1 [online], available from URL: www.seismosoft.com.

Shrestha, K.C., Saiidi, M.S. and Cruz, C.A. (2015). Advanced materials for control of post-earthqauke damage in bridges. *Smart Materials and Structures*, 24 (2015): 025035 (16pp).

Shrestha, K.C., Araki, Y., Takuya Nagae, T., Koetaka, Y., Suzuki, Y., Omori, T., Sutou, Y., Kainuma, R. and Ishida, K. (2013). Feasibility of Cu–Al–Mn superelastic alloy bars as reinforcement elements in concrete beams. *Smart Mater. Struct.* 22:025025 (12pp).

Tanaka, Y., Himuro, Y., Kainuma, R., Sutou, Y., Omori, T. and Ishida, K. (2010). Ferrous polycrystalline shape-memory alloy showing huge superelasticity. Science, 327:1488-1490.

Tehrani P and Mitchell D. Seismic response of bridges subjected to different earthquake types using IDA. *Journal of Earthquake Engineering*, 2013; **17**(3): 423-448.

Vamvatsikos, D. and Cornell, A. C. (2002). Incremental dynamic analysis. *Earthquake Engineering & Structural Dynamics*, 31, 491–514.